Applied Computer Science 2026, vol. 22, no. 2, pp. 85–104
https://doi.org/10.35784/acs_8936

Submitted: 2026-01-04 | Revised: 2026-05-05 | Accepted: 2026-05-07

Keywords: numerical investigation, blade angle, water vortex hydro turbine, computational fluid dynamics, CFD

Sarwo EDHY SOFYAN [1], *Zamzami* [2], *Akhyar AKHYAR* [1*], *Suriadi* [3], *Agus SASMITO* [4]

[1] Department of Mechanical Engineering, Universitas Syiah Kuala, Jln. Syech Abdurrauf No.7 Darussalam, Banda Aceh 23111, Indonesia, sarwo.edhy@usk.ac.id, akhyar@usk.ac.id

[2] Department of Electrical Engineering, Politeknik Negeri Lhokseumawe, Jl. Banda Aceh-Medan KM. 280 Buketrata, Lhokseumawe 24301, Indonesia, zamzami@pnl.ac.id

[3] Department of Electrical and Computer Engineering, Universitas Syiah Kuala, Banda Aceh 23111, Indonesia, suriadimali@usk.ac.id

[4] National Research and Innovation Agency of Indonesia, Jl. Hidrodinamika, Sukolilo, Surabaya 60112, Indonesia, agus107@brin.go.id

[*] Corresponding author: akhyar@usk.ac.id

Numerical investigation into the hydrodynamic characteristics of water vortex turbines with varied blade angles

Abstract

Water Vortex Hydro Turbines are a promising renewable energy solution for ultra-low-head applications, with performance strongly influenced by blade geometry in converting vortex-induced momentum into mechanical energy. This study numerically investigates the hydrodynamic characteristics including velocity distribution, air-core formation, and pressure gradient to determine the optimal blade angle using transient Computational Fluid Dynamics (CFD) with the Realizable k-ε turbulence model. A six-bladed turbine was analysed at blade angles of 75°, 90°, and 105° under a constant inlet velocity of 1 m/s. The results demonstrate that the 90° configuration delivers the best overall performance, with the maximum velocity increasing from 3.096 m/s (75°) to 4.376 m/s (90°), representing an improvement of approximately 41.4% and indicating a significantly stronger and more stable vortex structure. Although the 105° configuration reaches the highest peak velocity of 4.657 m/s, severe flow separation reduces flow stability and limits effective energy transfer. In terms of pressure, the 90° configuration produces the most favourable and symmetric gradient, with a maximum of 5777.397 Pa and a minimum of 3.154 Pa, compared to the more distorted distributions observed in the 75° and 105° cases (5741.087 Pa and 5892.066 Pa, respectively). Additionally, the 90° configuration generates a more compact and stable air-core, reducing hydraulic losses and enhancing fluid–blade interaction. Overall, the 90° blade angle provides the optimal balance between velocity magnitude, vortex stability, and pressure distribution, making it the most effective configuration for maximizing energy conversion in ultra-low-head water vortex hydro turbines.

1. INTRODUCTION

The utilization of renewable energy has become a global imperative, given the heavy reliance on fossil fuels that results in resource depletion and severe environmental repercussions, including global warming and pervasive pollution (Gayen et al., 2024). Electricity, as a vital necessity underpinning almost all human activities, must be supplied from sustainable sources. One relevant solution is the Hydropower Plant (HPP), which effectively converts the potential energy of water into electrical energy (Permana & Potipituk, 2024). Countries endowed with abundant water resources, including Indonesia, have great potential for hydropower development, particularly low-head systems (Zamzami et al., 2025a). In this context, the ultra-low-head water vortex reaction turbine has emerged as an innovative technology ideally suited for implementation in rivers or irrigation channels characterized by minimal current velocities and water height (head) (Zamzami et al., 2025a). Refining these turbines for low-head environments is essential to significantly enhance the potential for sustainable, ecologically sound exploitation of water resources, thereby underpinning the future provision of renewable energy (Lodhi et al., 2024).

Continuous efforts to improve the efficiency of vortex turbines are pursued through various experimental and numerical methods. One of the most effective approaches is via CFD, which allows for a detailed analysis of fluid flow behavior and turbulence around hydraulic structures (Xiaojing et al., 2023). In the application of vortex turbines, CFD is invaluable for modeling the flow, predicting the distribution of velocity, pressure, and kinetic energy, and analyzing the impact of design variations (such as blade geometry) on overall turbine performance (Edirisinghe et al., 2022; Firoozi et al., 2024; Frant et al., 2020). This virtual approach is highly efficient, enabling the testing of numerous scenarios without the need for physical prototype fabrication, thereby significantly saving costs and time (Hou et al., 2024; Ibrahim et al., 2022). Key basin design parameters, including water head, geometry, and the design of the inlet and outlet channels, are critical determinants of optimal performance (Kabat et al., 2022; Kan et al., 2023; Khoshkalam et al., 2020). The outlet diameter ratio adopted in this study was set to 0.2, placing it within the optimal range for generating a stable vortex (Ullah et al., 2020).

The primary focus of this research is to evaluate the influence of varying turbine blade-angle configurations on both hydrodynamic properties and energy conversion efficiency. These changes in blade angle configuration fundamentally affect three main aspects of the fluid flow within the turbine basin. Firstly, the blade angle configuration significantly influences the velocity distribution, which is the key determinant of vortex stability and quality (Li et al., 2020). A stable vortex with high tangential velocity is crucial for maximizing the momentum transfer and torque to the turbine blades (Li et al., 2023). Secondly, modifications to the blade-angle configuration influence the water volume-fraction distribution, which correlates directly with the compactness of the air core (air nucleus) and the fluid interaction at the vortex center (Wang et al., 2024). A stable, streamlined air core is necessary to mitigate cavitation and minimize energy losses from friction (Maika et al., 2023). Thirdly, the blade-angle configuration affects the pressure distribution, generating a pressure gradient and dictating the effectiveness of energy extraction. An optimal pressure gradient around the blades is the primary mechanism by which the turbine converts hydraulic energy into mechanical work (Maisuria et al., 2024). Based on this hydrodynamic analysis, the selected blade-angle configuration is projected to provide the ideal balance between lift and drag forces, yielding a stable vortex, a compact air core, and the most effective differential pressure gradient for energy extraction in ultra-low-head vortex turbines (Masoodi & Goyal, 2021).

Despite extensive research on GWVHTs, a critical knowledge gap remains regarding how blade-angle geometry simultaneously affects the velocity distribution, air-core formation, and pressure gradient under ultra-low-head conditions. Existing studies have largely addressed individual performance metrics without a unified, transient CFD-based analysis that captures both vortex stability and energy conversion behavior across systematically varied blade angles. Consequently, this study aims to conduct a transient CFD analysis using the Realizable k-ε turbulence model to evaluate six blade-angle configurations (75°, 90°, and 105°), with the objective of identifying the optimal design to enhance hydrodynamic performance in ultra-low-head Water Vortex Hydro Turbines.

2. PROCECDURE

Water vortex turbines have attracted considerable attention from researchers and engineers due to their potential to convert water's kinetic energy into electricity without requiring large dams or causing significant environmental impact. Conceptually, this turbine harnesses the centrifugal force of water within a vortex system to drive the rotor blades' rotation (Varga et al., 2025). This makes it a promising solution for sustainable energy production, particularly in environments with low or ultra-low headwater flow, where traditional turbines cannot operate effectively.

The Gravity Water Vortex Hydro Turbine (GWVHT) system typically consists of a water inlet channel, a circular basin with a bottom aperture serving as the water outlet, and a rotor equipped with several blades connected to a vertical shaft (Pędzisz et al., 2024). By harnessing the natural flow of water, this system generates a free-surface vortex that improves water circulation and induces a pressure drop at its center, thereby creating an air core (Domfeh et al., 2020). Energy conversion occurs when the mechanical energy from the blade rotation is transferred to an attached generator.

A crucial aspect of the GWVHT is the strength of the free-surface vortex, which directly determines the turbine's efficiency. A free vortex refers to an area of flow where no external driving force, other than gravity, influences the flow dynamics. The free-surface vortex in a GWVHT is identified as having several distinct

layers: the air-core formed at the vortex center, the region between the water surface and the free vortex, the region between the forced vortex and the water boundary layer near the basin wall, and the water near the wall that is affected by friction (Seng & Tanjong, 2025). The design and optimization of the vortex turbine are therefore crucial for maximizing energy yield.

In this study, the CFD approach was employed to investigate the hydrodynamic behavior of the vortex turbine, formulated based on the Navier–Stokes equations (1–4) (Sonawat et al., 2020; Sukadana et al., 2024).

$$\frac{\partial V_r}{\partial r}+\frac{\partial V_z}{\partial z}+\frac{V_r}{r}=0 \tag{1}$$

$$V_r\frac{\partial V_\theta}{\partial r}+V_z\frac{\partial V_\theta}{\partial z}-\frac{V_r V_\theta}{r}=\nu\left(\frac{\partial^2 V_\theta}{\partial r^2}+\frac{\partial V_\theta}{r\partial r}-\frac{V_\theta}{r^2}+\frac{\partial^2 V_\theta}{\partial z^2}\right) \tag{2}$$

$$V_r\frac{\partial V_r}{\partial r}+V_z\frac{\partial V_r}{\partial z}-\frac{V_\theta^2}{r}+\frac{\partial \rho}{\rho\partial r}=\nu\left(\frac{\partial^2 V_r}{\partial r^2}+\frac{\partial V_r}{r\partial r}-\frac{V_r}{r^2}+\frac{\partial^2 V_r}{\partial z^2}\right) \tag{3}$$

$$V_r\frac{\partial V_z}{\partial r}+V_z\frac{\partial V_z}{\partial z}+\frac{\partial \rho}{\rho\partial z}=g+\nu\left(\frac{\partial^2 V_z}{\partial r^2}+\frac{\partial V_z}{r\partial r}+\frac{\partial^2 V_r}{\partial z^2}\right) \tag{4}$$

where V_r is the radial velocity, V_z is axial velocity, V_θ is the tangential velocity, ν is the kinematic viscosity, ρ is the fluid density, and g is gravitational acceleration.

The flow behavior and rotational forces in a vortex turbine can be described using the circulation parameter (Γ), which is expressed as:

$$\Gamma=2\pi r V_\theta \tag{5}$$

where Γ is the circulation parameter (m^2/s), r represents the distance from the center of rotation (m), and V_θ denotes the tangential velocity (m/s).

The tangential velocity (V_θ) observed in the vortex flow pattern is governed by the relationship between the radius and the fluid's viscosity. The value of V_θ at the inlet section of the generator (or basin) can be evaluated through the application of the continuity equations (6) and (7).

$$V_\theta=\frac{Q}{bh_{in}} \tag{6}$$

$$\Gamma=\frac{2\pi rQ}{bh_{in}} \tag{7}$$

where b denotes the width of the inlet channel, and h_{in} represents the depth of water at the inlet section.

The CFD simulations for this hydrodynamic investigation were performed using Ansys 19.2. The Ansys Fluent solver was used to perform transient (unsteady) simulations. The selection of Fluent was based on its superior capability to handle rotational flow and turbulence, using the Volume of Fluid (VOF) model to accurately track the air-water interface. This capability is crucial for precisely modeling the formation of the turbine's vortex air-core.

The turbine model simulated for this investigation was designed using the drawing application. This vortex turbine has primary dimensions of 1.5 meters in diameter and 1.38 meters in height. The system comprises a single water inlet channel and a single outlet (draft) tube. The main channel dimensions were: Inlet Channel (Length 1.8 m, Width 0.8 m, Height 1.2 m, with a bend angle of 146°); and the Outlet Channel (Draft Tube) (Diameter 0.75 m and Height 0.5 m).

The turbine rotor was designed with a fixed number of six blades. The blade geometry has standard dimensions: a shaft diameter of 0.1 m, a blade height of 0.35 m, a blade length of 0.3 m, and a thickness of 0.005 m. The parameter systematically varied in this study was the blade angle, tested at three configurations: 75°, 90°, and 105°. This study aims to evaluate the effects of blade-angle variations on hydrodynamic characteristics, including velocity distribution, pressure field, and flow behavior (Figures 1 and 2).

The selection of the blade angle configurations, specifically 75°, 90°, and 105°, was informed by preliminary studies indicating that this range encompasses the most favorable operating conditions for vortex turbines with comparable diameter ratios. This range concurrently offers two systematic extremes (one flatter and the other more upright) to facilitate a comparative analysis of the influence of water flow momentum

(Sharma, et al., 2021). Specifically, the 90° angle represents the standard perpendicular blade configuration relative to the axial flow. In contrast, the ± 15 ° variations (i.e., 75° and 105°) were judiciously chosen to systematically examine the turbine's performance sensitivity to moderate deviations from this standard configuration. Although a broader parametric sweep could yield more exhaustive optimization, the selected configurations are considered sufficient to identify dominant trends and the underlying physical mechanisms governing rotor-vortex interaction.

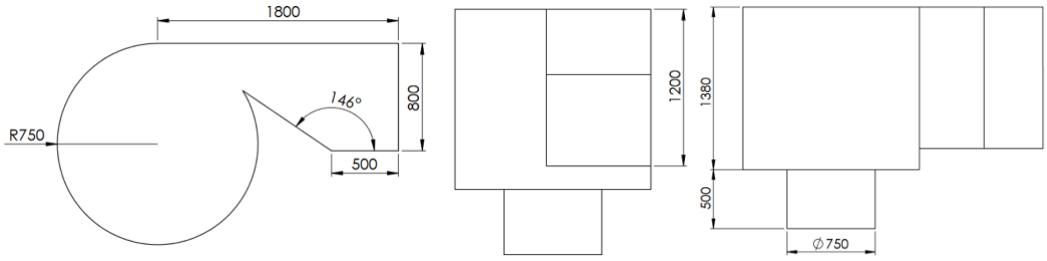

Fig. 1. Dimensions of the turbine blade with 3 blades (in mm)

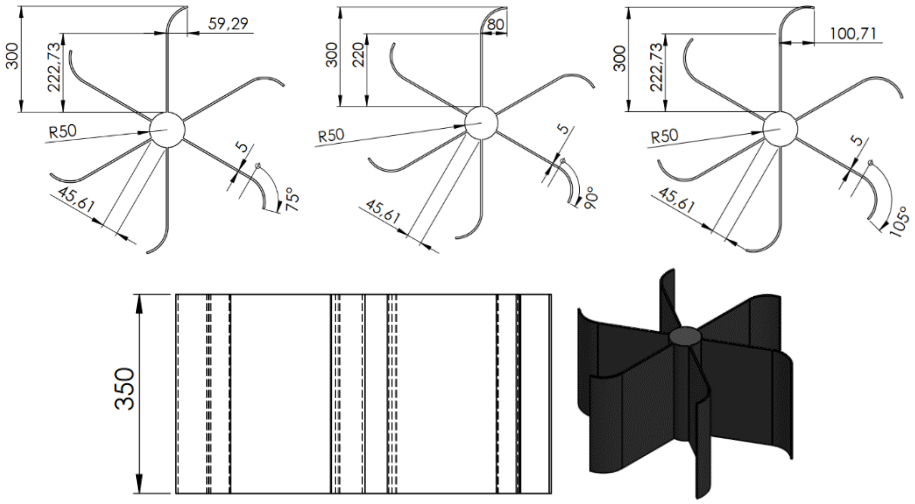

Fig. 2. Dimensions of the 6-bladed turbine, featuring blade angles of 75°, 90°, and 105° (in mm)

The domain discretization process, known as meshing, was performed after importing the geometry into DesignModeler (Figure 3). A tetrahedral mesh was employed because of its superior ability to handle complex geometries and its effectiveness in fluid flow analysis. The mesh size was set uniformly to 5 mm. Prior to running the CFD simulation, the mesh quality was evaluated, focusing on skewness and orthogonality. The resultant grid had a maximum skewness of 0.2 and an average orthogonality greater than 0.8, indicating that the elements were well-shaped and appropriate for accurate flow-field prediction. To ensure the accuracy of the near-wall flow physics, the mesh resolution was carefully controlled to satisfy the requirements of the Standard Wall Functions. The resulting area-weighted average y^+ value on the blade surfaces was maintained between 45 and 85. This y^+ range is well-positioned within the log-law region ($30 < y^+ < 300$), validating the compatibility between the mesh density and the Realizable k-ε turbulence model without the need for additional explicit inflation layers. The simulation was executed using a pressure-based, double-precision solver in transient mode with a time-step size of 0.005 s, a total of 600 time steps, and a maximum of 50 iterations per time step. The angular velocity was set to 7.2 rad/s. The numerical solution scheme applied was SIMPLE with Standard Initialization. Gravity was enabled with a value of 9.81 m/s^2, and the velocity formulation was set as absolute. The Volume of Fluid (VOF) model was activated, utilizing two Eulerian phases: Water (water-liquid) and Air, alongside an implicit body force formulation. The Realizable k-ϵ turbulence model was used, with standard wall functions applied for near-wall treatment.

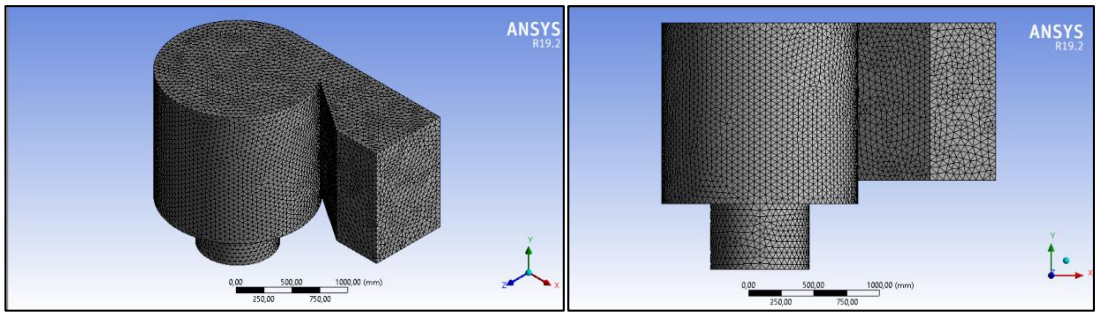

Fig. 3. Vortex chamber meshing result

The boundary conditions for the simulation were as follows: the inlet was set to a velocity-inlet condition under transient conditions, with a constant water entry velocity of 1 m/s (Figure 4), and the water volume fraction was set to 1. The inlet velocity of 1 m/s was selected based on the physical operating range of ultra-low-head WVHTs. For the inlet channel dimensions used in this study (width b = 0.8 m, water depth h_in = 1.2 m), this velocity corresponds to a volumetric flow rate of Q = 0.96 m^3/s, which is consistent with documented operating conditions for comparable vortex basin configurations (Shamsuddeen et al., 2023). The velocity-inlet boundary condition was adopted in preference to a pressure-inlet or mass flow formulation because this study undertakes a controlled parametric comparison of blade angle configurations; prescribing a uniform inlet velocity ensures all six blade angle cases (75°, 90°, and 105°) are evaluated under identical upstream flow conditions, enabling a rigorous and unambiguous assessment of geometric effects on hydrodynamic performance. The outlet was set to a pressure-outlet type with a specified static pressure. All walls, including the sides and floor, were designated as no-slip walls with standard conditions, being treated as solid and impermeable. The free surface between air and water was captured using the VOF method. These detailed settings for the initial conditions, boundary conditions, and geometric dimensions form the foundation of the numerical calculations used to investigate the vortex turbine's performance across a range of blade angles. The solution at each time step was considered converged when all residuals fell below the specified threshold of 0.001, with the maximum number of iterations limited to 50.

Rotor rotation in this study was modeled using a transient sliding mesh approach to accurately capture the interaction between the rotating blades and the free-surface vortex flow. The computational domain was divided into a rotating zone enclosing the rotor and a stationary fluid region, connected through a sliding interface that allowed the mesh to physically rotate and resolve unsteady flow structures. This method was selected over the Multiple Reference Frame (MRF) approach because it can capture time-dependent vortex dynamics, free-surface deformation (via the VOF method), and rotor-flow interactions more realistically, providing a more accurate representation of the turbine's hydrodynamic behavior.

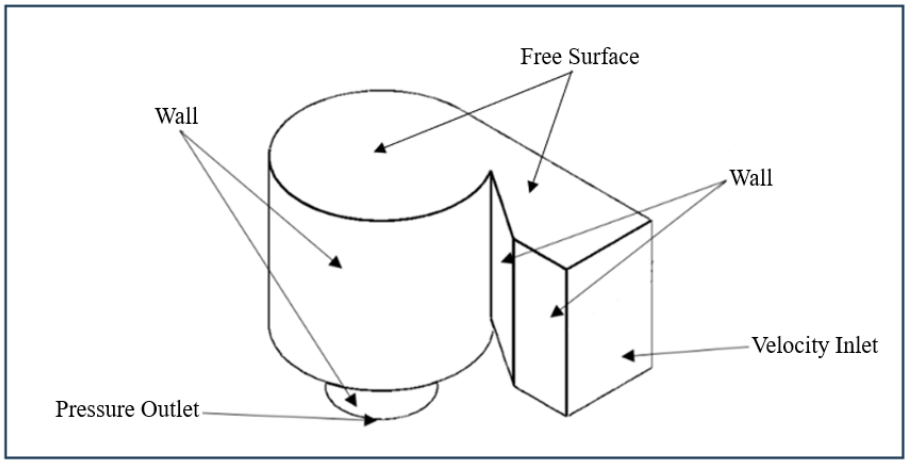

Fig. 4. Boundary conditions of the Vortex chamber

A mesh sensitivity analysis was conducted to assess the effect of grid resolution on the computational accuracy of the CFD simulation of the Water Vortex Hydro Turbine (WVHT), as shown in Figure 5. The analysis focused on the blade tangential velocity as the primary performance parameter, since it directly

represents the turbine's hydrodynamic behavior and energy extraction characteristics. Five mesh densities were examined, corresponding to 9,207,751; 12,597,443; 17,802,969; 28,940,594; and 53,124,783 nodes. The results indicate that the blade tangential velocity remains nearly constant across all mesh resolutions, with values around 1.285 m/s and only a very slight decrease at the finest mesh. The variation is minimal, demonstrating that the solution is not significantly affected by further mesh refinement. Beyond approximately 17 million nodes, the changes in velocity become negligible, indicating that the solution has reached a mesh-independent region. Therefore, the mesh with around 17,802,969 nodes can be considered optimal, as it provides a good balance between computational cost and numerical accuracy. The small discrepancies observed at higher mesh densities may be attributed to numerical diffusion or local flow-resolution effects. Overall, the mesh sensitivity analysis confirms that the CFD model yields stable, reliable results once the mesh size exceeds approximately 17 million nodes.

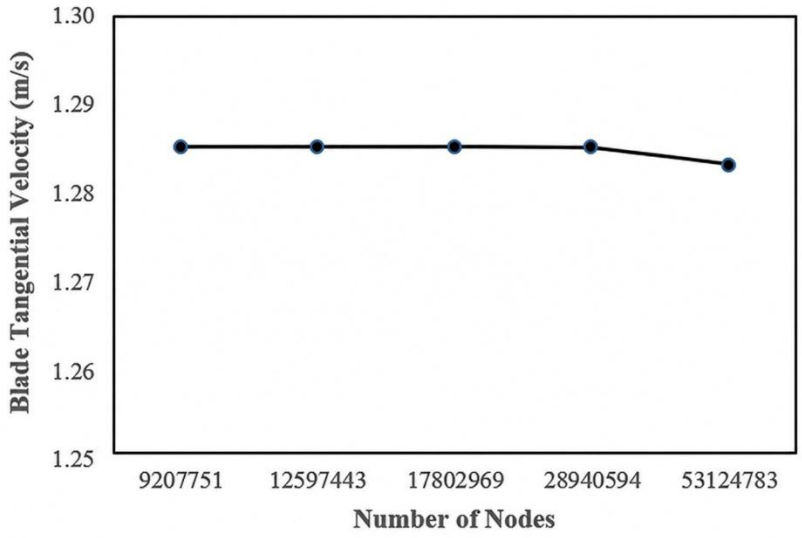

Fig. 5. Mesh sensitivity analysis showing the effect of the number of nodes on blade tangential velocity for the Water Vortex Hydro Turbine

Blade tangential velocity was adopted as the key performance indicator in the mesh sensitivity assessment of the WVHT, as it effectively represents the turbine's hydrodynamic response and its ability to convert vortex flow energy into mechanical output. The evaluation was performed using five mesh resolutions, spanning from 9,207,751 to 53,124,783 nodes, as illustrated in Figure 5. The findings reveal a high level of solution consistency, with blade tangential velocity remaining nearly unchanged across all mesh configurations, fluctuating only within the narrow range of approximately 1.284–1.285 m/s. A marginal reduction is observed at the finest mesh; however, this variation is insignificant. It is evident that beyond approximately 17,802,969 nodes, the velocity variation becomes negligible, indicating convergence to a mesh-independent solution. This asymptotic behavior confirms the robustness and numerical stability of the CFD model. Accordingly, the mesh containing approximately 17,802,969 nodes is considered optimal, as it achieves an effective balance between computational efficiency and solution accuracy. In general, mesh refinement beyond this threshold does not yield substantial improvements in the predicted blade tangential velocity.

The predicted blade tangential velocity of 1.28 m/s shows excellent agreement with published data. Previous studies have reported tangential velocity values in the range of 1.1-1.4 m/s for similar GWVT configurations (Edirisinghe et al., 2022). Using a representative reference value of 1.25 m/s, the deviation of the present result is approximately 2.4%, indicating a very good level of accuracy. This small deviation confirms that the present CFD model accurately captures the hydrodynamic behavior of the vortex flow and provides reliable predictions.

Theoretical framework for hydrodynamic evaluation: to evaluate the numerical results, the vortex flow is characterized by the Rankine vortex model, in which the tangential velocity (v_t) and the pressure distribution (P) are governed by the conservation of angular momentum. The theoretical pressure drop (ΔP) across the turbine blades, which drives the mechanical torque, can be estimated using Euler's turbine equation:

$$\Delta P \approx p.(u_1 v_{t1} - u_2 v_{t2}) \quad (8)$$

where ρ is the water density, u is the blade tangential velocity, and v_t is the fluid tangential velocity. Furthermore, the air-core formation (water volume fraction) is theoretically linked to the Bernoulli principle, where the pressure at the vortex center (P_c) must drop below atmospheric pressure (P_{atm}) to form a void:

$$P_c = P_{atm} - \int \rho \frac{v_t^2}{r} dr \quad (9)$$

These equations provide the basis for understanding why variations in blade angle (75°, 90°, and 105°) (which alter the velocity triangles and momentum exchange) directly result in the pressure and volume fraction distributions observed in the CFD contours.

3. RESULTS AND DISCUSSION

This simulation undertakes a comprehensive analysis of the Hydro-Vortex Water Turbine hydrodynamic characteristics, focusing specifically on the evaluation of velocity distribution, water volume fraction, and pressure gradient across six distinct blade angle configurations: 75°, 90°, and 105°. These three critical parameters exhibit an intrinsic and profound correlation; the stability of the generated vortex, as quantified by the velocity distribution profile, fundamentally governs the compactness of the resulting air nucleus. Subsequently, this compactness dictates the differential pressure drop that can be efficiently extracted, determining the overall energy extraction effectiveness.

3.1. Velocity distribution

Figure 6 illustrates the velocity contours for the 75° vane angle. The discussion of these CFD simulation results is framed in the context of a configuration that yields less favorable flow characteristics. As the water enters the zone above the turbine, it displays a variable velocity distribution, predominantly ranging from 1.548 m/s (green) to 3.096 m/s (yellow). However, despite the initial vortex formation, the flow stability generated by the 75° angle remains characteristically low. This instability is evidenced by the clear nonuniformity of the velocity contours within the draft tube. Rather than forming a dense, symmetric vortex ring, the velocity pattern appears fragmented and highly distorted, clearly indicating an unstable vortex structure. This lack of stability is further corroborated by the observation of significantly low-velocity regions (light blue to green, ranging from 0 m/s to 1.548 m/s) in specific peripheral and upstream sections of the draft tube.

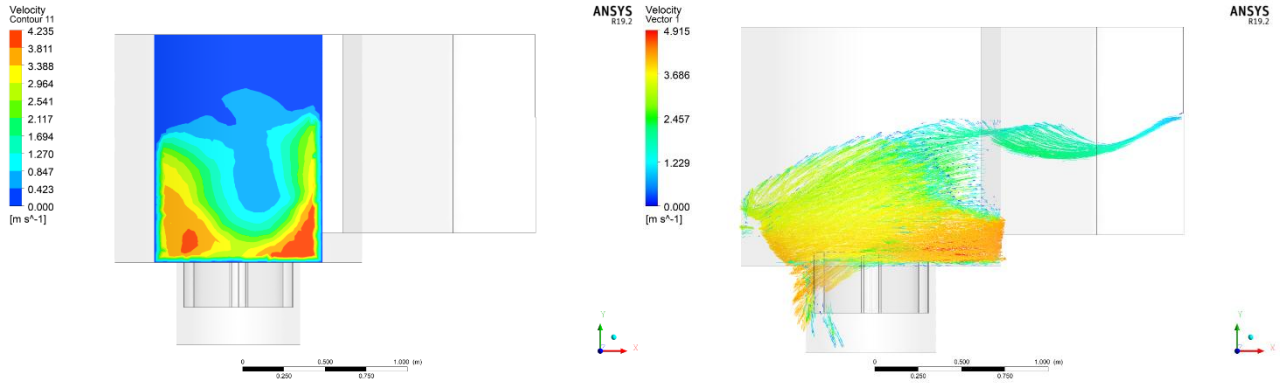

Side vertical XY cross section **Vector velocity side view**

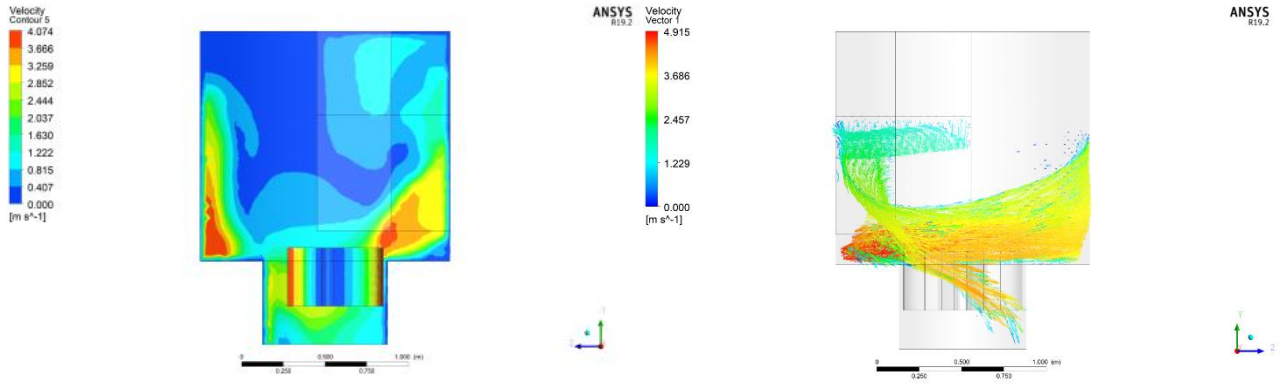

Front vertical YZ cross section (0.6 m from the front) **Front velocity vector**

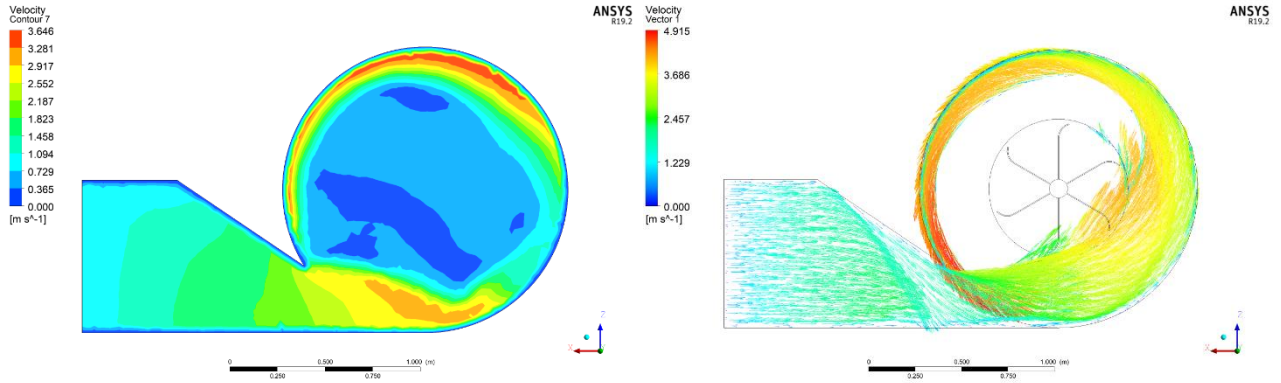

Middle horizontal XZ section (0.9 m from top) **Vector velocity top view**

Fig. 6. Velocity distribution of the vortex chamber at 75° blade angle (various cross-sections)

The presence of these extensive low-velocity areas suggests either recirculation zones or regions where vortex momentum has not been fully developed. This condition directly contributes to substantial hydraulic losses. Consequently, the uneven velocity distribution indicates that the turbine blades have not efficiently converted the tangential energy into mechanical energy. This inability to sustain a powerful, symmetric vortex is the underlying reason the 75° configuration results in less effective flow conditions for energy transfer within the turbine.

Figure 7 presents the velocity contours for the 90° blade-angle configuration, designated in this numerical study as the optimal design. Visually, the velocity contours depicted in Figure 7 confirm superior hydrodynamic performance.

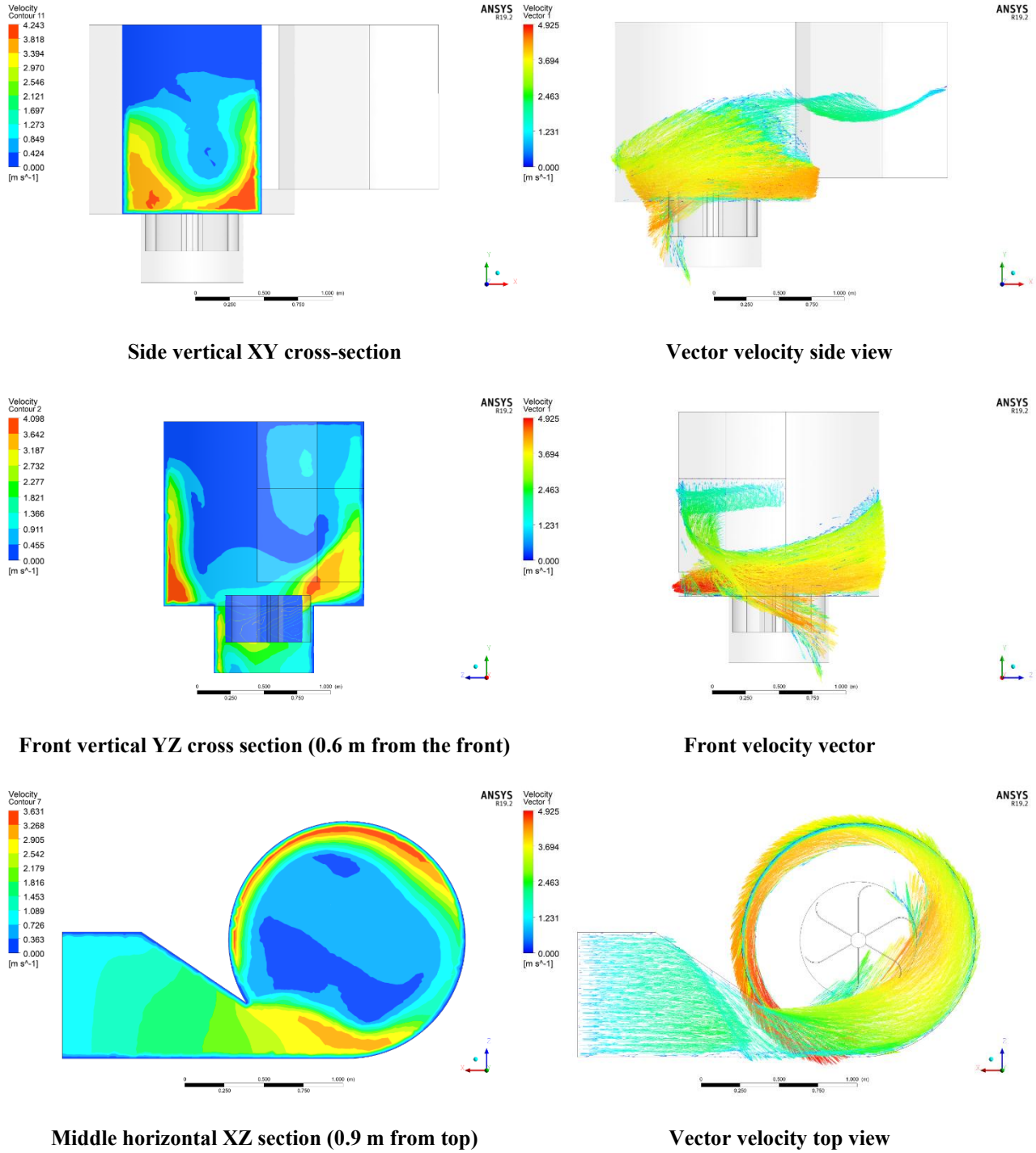

Side vertical XY cross-section **Vector velocity side view**

Front vertical YZ cross section (0.6 m from the front) **Front velocity vector**

Middle horizontal XZ section (0.9 m from top) **Vector velocity top view**

Fig. 7. Velocity distribution of the vortex chamber at 90° blade angle (various cross-sections)

The observed flow exhibits stable, highly uniform characteristics, in sharp contrast to the instability observed at the 75° angle. The high-velocity flow regions, indicated by bright yellow (3.063 m/s) extending to deep red (4.376 m/s), appear dense and highly symmetrical within the draft tube area. This distinctive pattern unequivocally indicates the formation of a strong, stable vortex (a compact vortex ring), a critical condition for minimizing hydraulic power losses. The maximum velocity is 4.376 m/s, indicating a highly efficient conversion of potential energy into kinetic energy before the fluid interacts with the turbine blades. Furthermore, the velocity distribution across the entire vertical cross-section tends to be balanced and highly

uniform, substantiated by the minimal presence of large, very low-velocity areas (0 m/s to 0.438 m/s) within the main flow region. This outcome indicates that a stable vortex flow is successfully maintained down to the turbine's lower section. This stable and uniform flow quality is fundamental to achieving the highest energy extraction effectiveness, as it guarantees that the maximum effective pressure differential (the optimal pressure gradient) can be attained along the vanes, thereby facilitating maximal fluid mass interaction.

Figure 8 displays the velocity contour pattern, confirming that the 105° blade angle results in a significant performance degradation due to severe hydrodynamic issues. The velocity distribution around the draft tube and upstream of the blades appears diffuse and unstable. Crucially, the high-velocity flow (ranging from 3.260 m/s to 4.657 m/s) fails to produce the compact vortex ring observed in the 90° configuration. A critical phenomenon observed is premature flow separation, which is indicated by the substantial expansion of low-velocity areas (blue color, 0 m/s to 1.397 m/s) along the periphery of the draft tube.

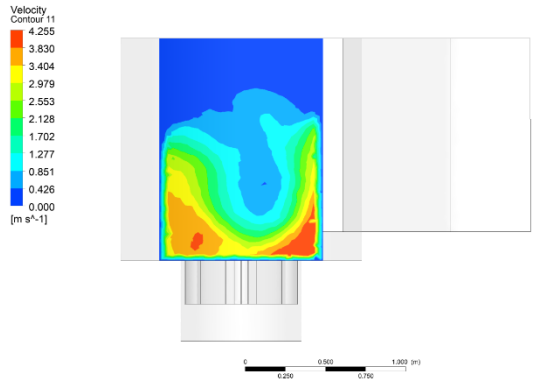

Side vertical XY cross section

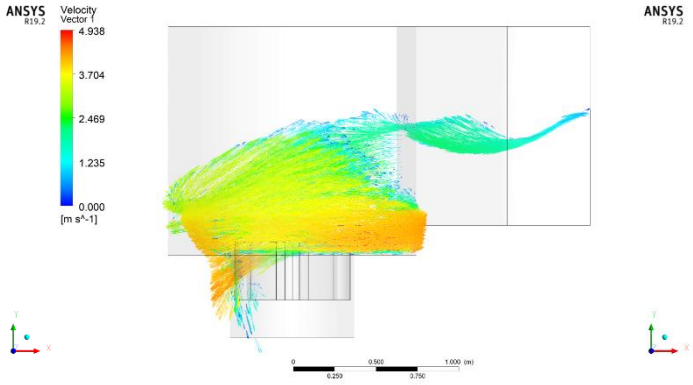

Vector velocit side view

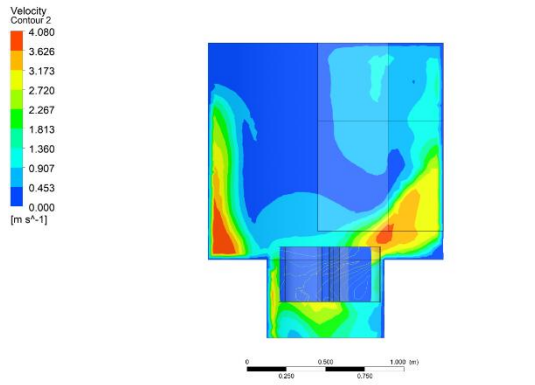

Front vertical YZ cross section (0.6 m from the front)

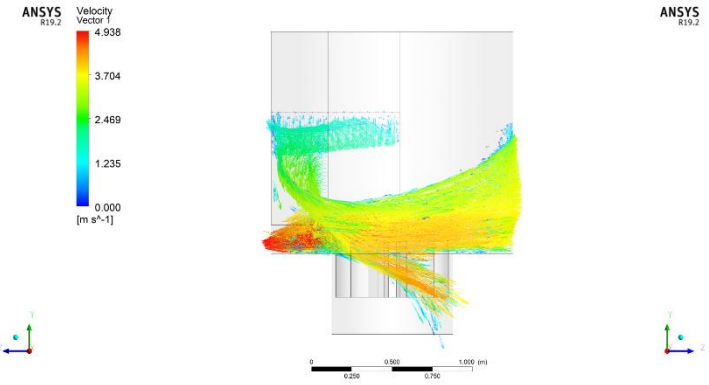

Front velocity vector

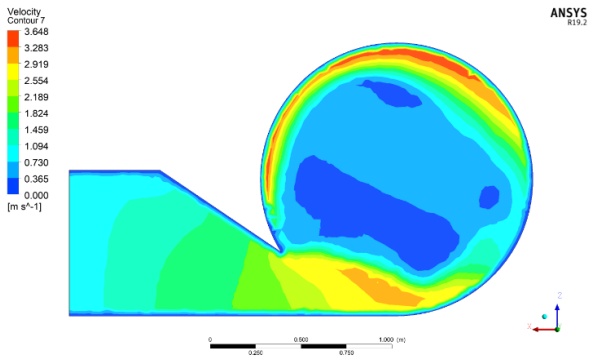

Middle horizontal XZ section (0.9 m from top)

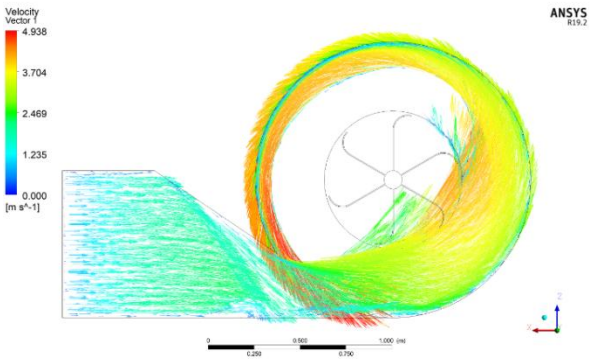

Vector velocit top view

Fig. 8. Velocity distribution of the vortex chamber at 105º blade angle (various cross-sections)

This flow separation subsequently results in the formation of large low-velocity pockets (recirculation zones) and a thickened boundary layer (an enlarged wake) downstream of the vanes. The direct hydraulic consequence is a distortion of the pressure pattern and increased hydraulic losses, as the vortex energy cannot be efficiently transferred to the blades. The non-uniform and diffuse velocity contours indicate an inability to sustain the required vortex compactness, thereby diminishing the differential pressure gradient along the vanes and ultimately lowering the turbine's overall performance. This flow pattern conclusively establishes the 105 ° configuration as an unfavorable, suboptimal design.

3.2. Water volume fraction distribution

The analysis of the water volume fraction corroborates the velocity distribution results, demonstrating that vortex stability is directly related to the geometry of the air nucleus. The compactness of this air nucleus is crucial, as a slender central area ensures maximum effective fluid-mass interaction with the turbine vanes.

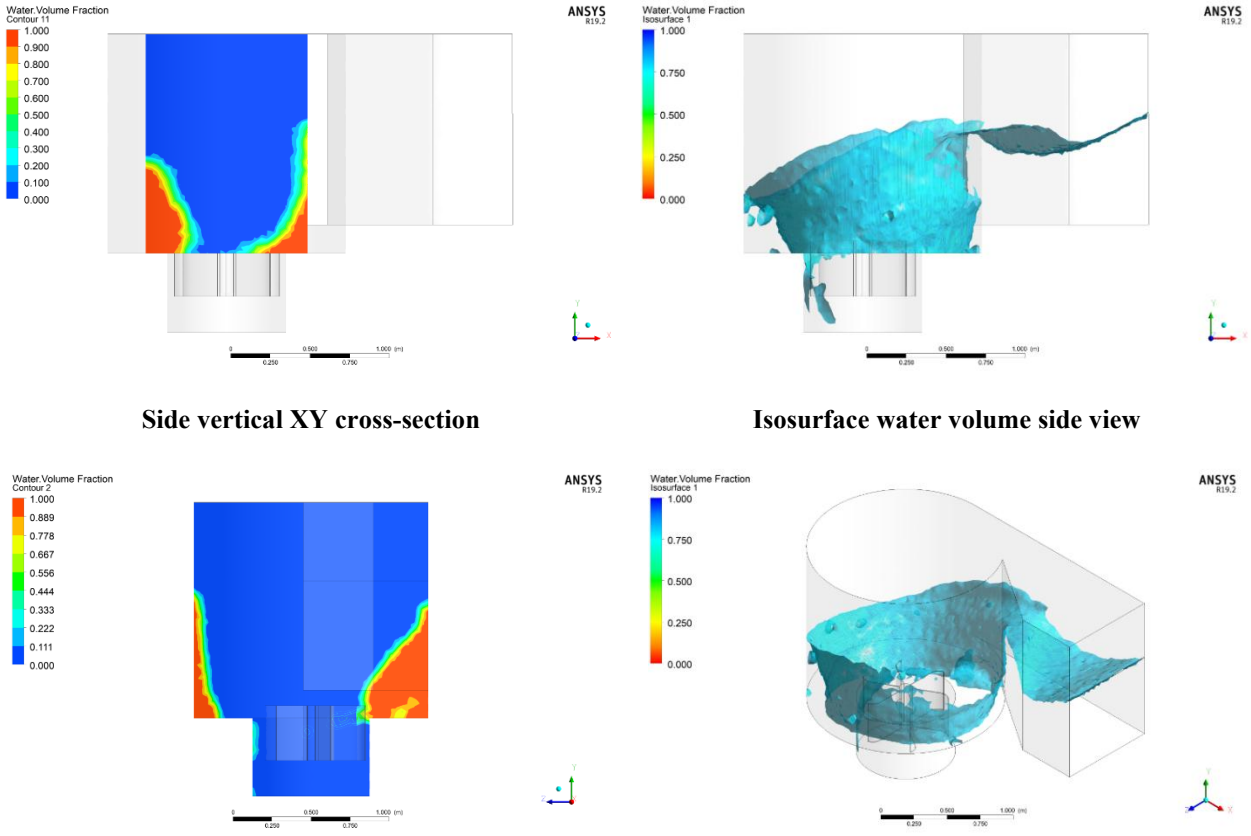

Side vertical XY cross-section **Isosurface water volume side view**

Front vertical YZ cross section (0.6 m from the front) **Isosurface water volume fraction 3D view**

Middle horizontal XZ section (0.9 m from top) **Isosurface water volume top view**

Fig. 9. Water volume distribution of the vortex chamber at 75° blade angle (various cross-sections)

Figure 9 illustrates the unstable water volume distribution at the 75° angle, aligning with the previously noted unfavorable flow characteristics. Consistent with the preceding study outcomes, this configuration produces a relatively wide air nucleus (blue area, 0 water volume fraction). The air nucleus formed in the upper section of the draft tube appears both expanded and unfocused. Furthermore, the boundary of the water's free surface (the transition between fractions 0.111 and 0.889) exhibits a wavy, highly asymmetrical pattern. This non-uniformity indicates that the resulting vortex is unstable and poorly controlled, a direct consequence of the fragmented velocity profile. The negative hydrodynamic consequences are twofold: Firstly, the expanded air nucleus significantly reduces the effective contact area between the swirling water and the turbine blades, thereby limiting the potential for maximum energy extraction effectiveness. Secondly, the vortex instability, evidenced by the irregular shape of the air nucleus, leads to greater hydraulic energy losses, indicating reduced effectiveness of momentum transfer within the flow.

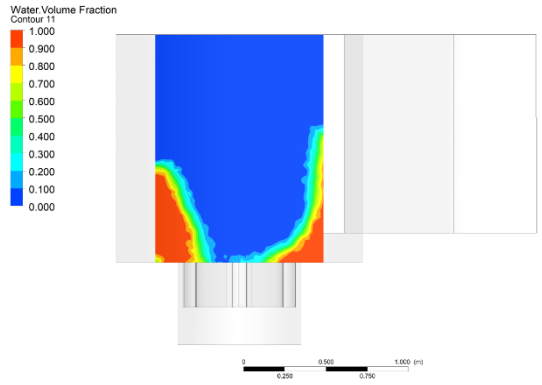

Side vertical XY cross section

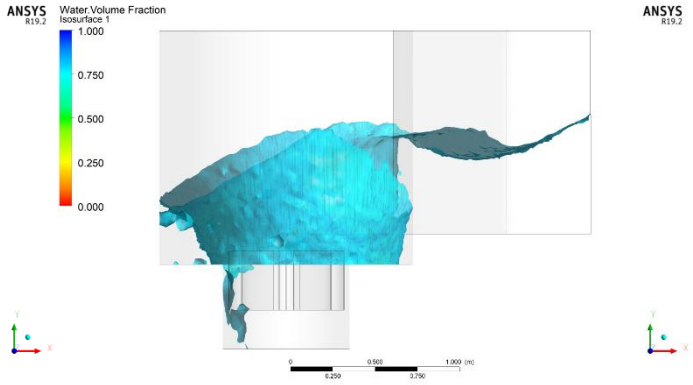

Isosurface water volume side view

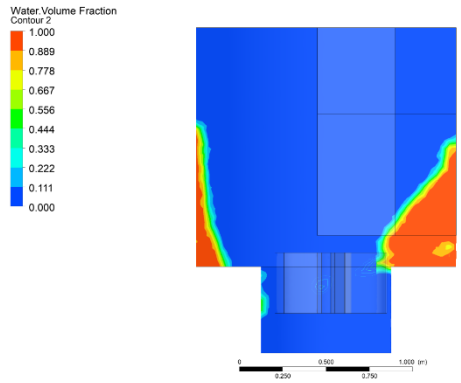

Front vertical YZ cross section (0.6 m from the front)

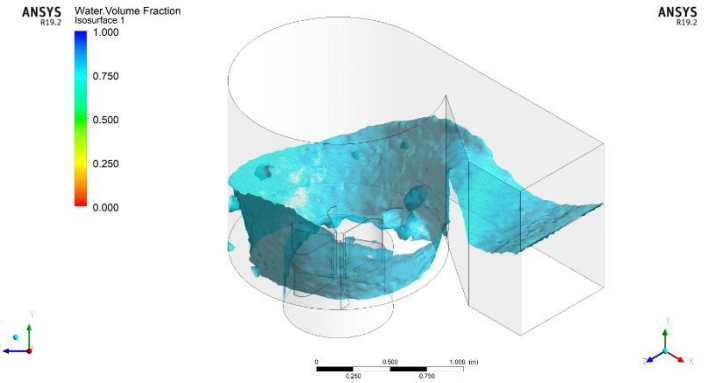

Isosurface water volume 3D view

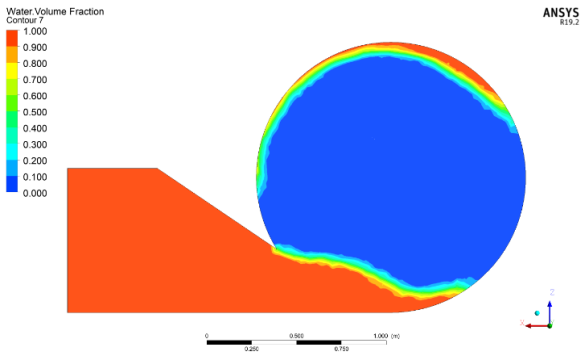

Middle horizontal XZ section (0.9 m from top)

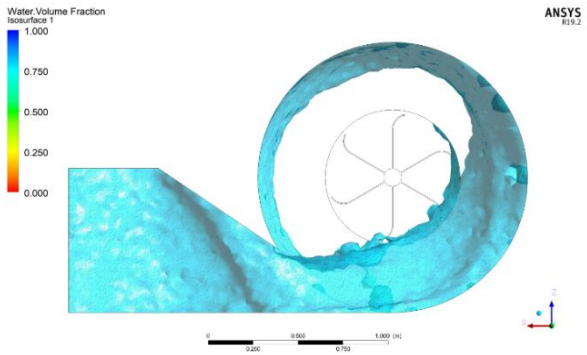

Isosurface water volume top view

Fig. 10. Water volume distribution of the vortex chamber at 90° blade angle (various cross-sections)

Figure 10 illustrates the water volume distribution at 90°, providing strong support for the findings of optimal hydrodynamic performance and maximum energy extraction efficiency. The water volume pattern shows a slender, highly focused air nucleus (blue area, 0 water volume fraction) that forms symmetrically at the vortex center. In stark contrast to the 75° configuration, the boundary line of the water's free surface in Figure 10 (the transition between fractions 0.100 and 0.900) appears smoother and highly consistent. This pattern substantiates the creation of a strong, stable vortex with minimal power loss. This vortex compactness is of paramount importance because the slender air nucleus ensures maximum effective interaction of the fluid mass with the vanes. The majority of the swirling water volume (1.000 fraction) remains in effective contact with the blades, thereby enabling optimal energy conversion. This condition is a key determinant of enhanced fluid–blade interaction and reduced hydrodynamic losses, thereby firmly validating this design recommendation.

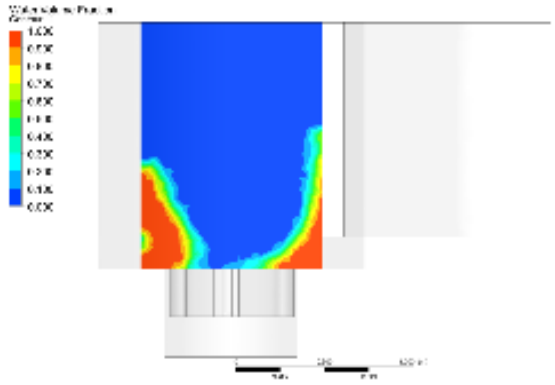

Side vertical XY cross-section

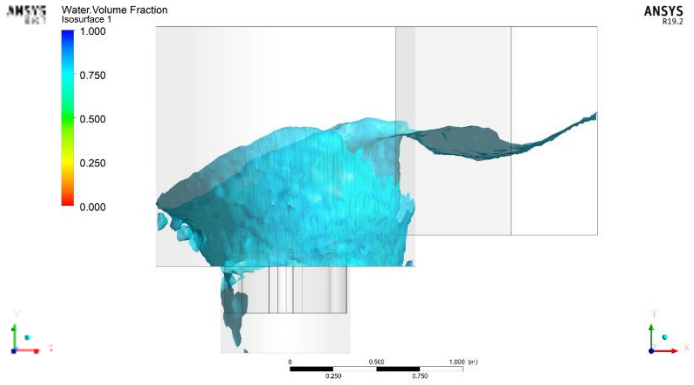

Isosurface water volume side view

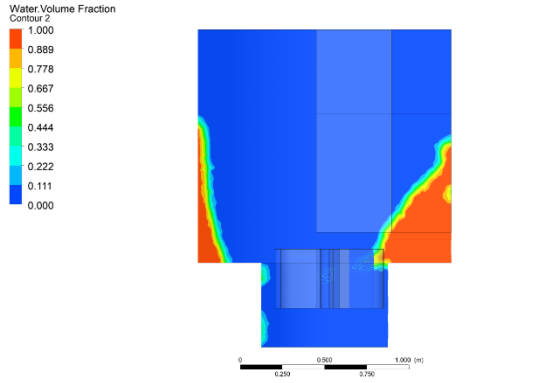

Front vertical YZ cross section (0.6 m from the front)

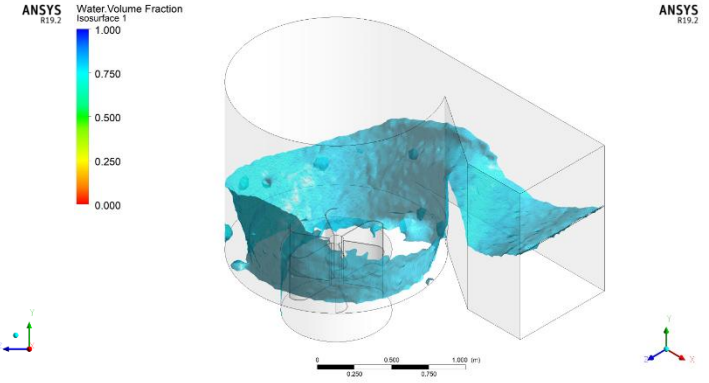

Isosurface water volume 3D view

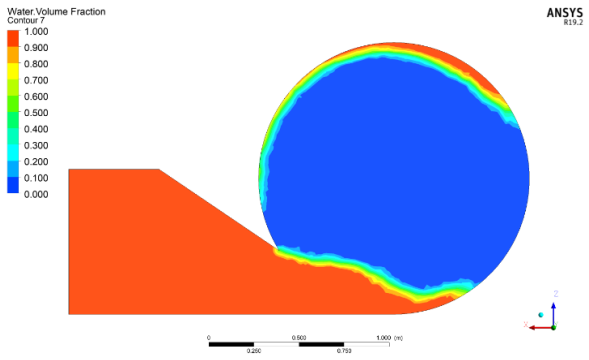

Middle horizontal XZ section (0.9 m from top)

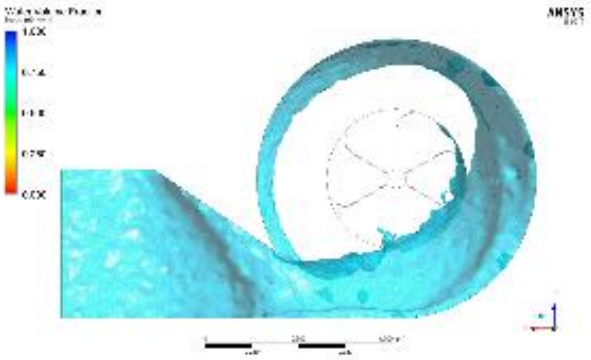

Isosurface water volume top view

Fig. 11. Water volume distribution of the vortex chamber at 105° blade angle (various cross-sections)

Figure 11 further corroborates the findings of hydrodynamic distortion at the 105° angle. The air nucleus area (blue region, 0 water volume fraction) appears expanded and exhibits a highly irregular boundary pattern. This outcome aligns with studies stating that, hydraulically, the air nucleus widens at this specific angle. The boundary line of the water's free surface (the transition between fractions 0.100 and 0.900) displays significant undulations and non-uniformity, confirming that the resulting vortex is both unstable and severely distorted. The expansion of the air nucleus depicted in Figure 11 is directly attributable to premature flow separation, which effectively diminishes the volume of water interacting with the vanes. Consequently, this leads to increased hydraulic losses and reduced effectiveness of momentum transfer. This unstable, widened water-volume pattern strongly reinforces the conclusion that the 105° configuration is a suboptimal design.

3.3. Pressure distribution

The pressure distribution analysis reveals the differential pressure gradient along the vanes. Fundamentally, this gradient generates the thrust force acting upon the turbine blades.

Figure 12 displays the pressure contours at the 75° angle, thereby reinforcing the conclusion of non-uniform pressure distribution.

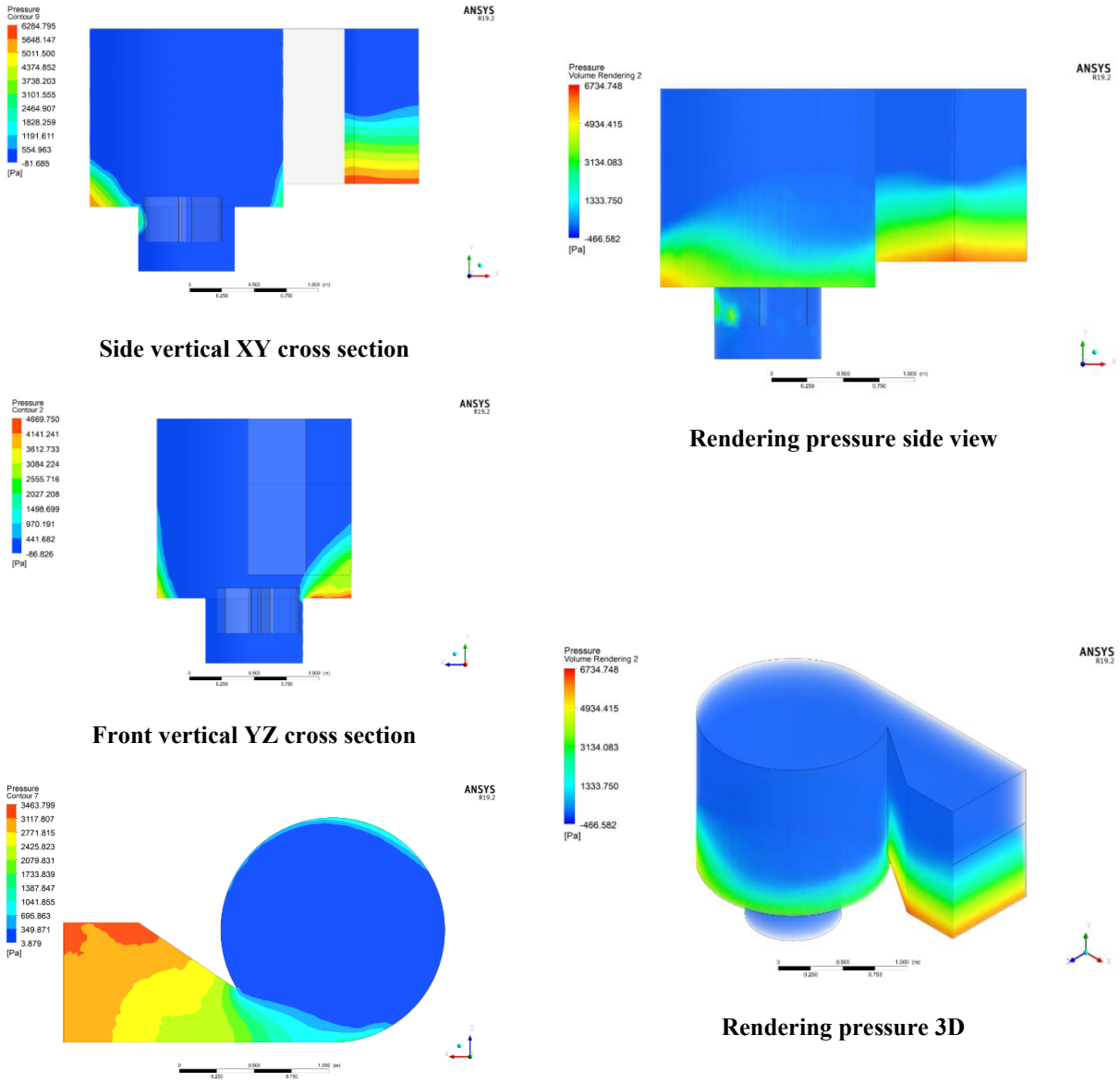

Fig. 12. Pressure distribution of the vortex chamber at 75° blade angle (various cross-sections)

The maximum pressure, reaching 5741.087 Pa (deep red), is concentrated in the lower section of the draft tube and immediately upstream of the vanes. While this high pressure indicates initial thrust potential, the resulting pressure gradient is asymmetric. After passing the blades, the pressure rapidly drops towards the minimum value of 6.720 Pa, suggesting a suction effect. This asymmetry in the pressure pattern is a direct manifestation of the unstable vortex and the widened air nucleus, both of which hinder the development of a consistent, maximum pressure differential between the pressure and suction sides of the vanes. The consequence is that the tangential energy has not been fully or effectively converted, which ultimately results in less effective momentum transfer within the flow.

The 90° configuration exhibits the most favorable pressure distribution pattern (Figure 13). The maximum pressure, at 5777.397 Pa (deep red), is concentrated uniformly within the draft tube area, ensuring that the fluid exerts maximum thrust on the pressure side of the vanes. The key quality resides in the gradient established following the vane interaction. The pressure drops drastically to a minimum of 3.154 Pa (deep blue) on the suction side, indicating highly effective energy extraction by the blades and a large differential pressure drop. These pressure contours display a consistent, symmetrical pattern around the blade area, indicative of a stable vortex flow. This optimal, symmetrical pressure pattern indicates the absence of flow distortion, thereby supporting effective momentum transfer across the blade surfaces.

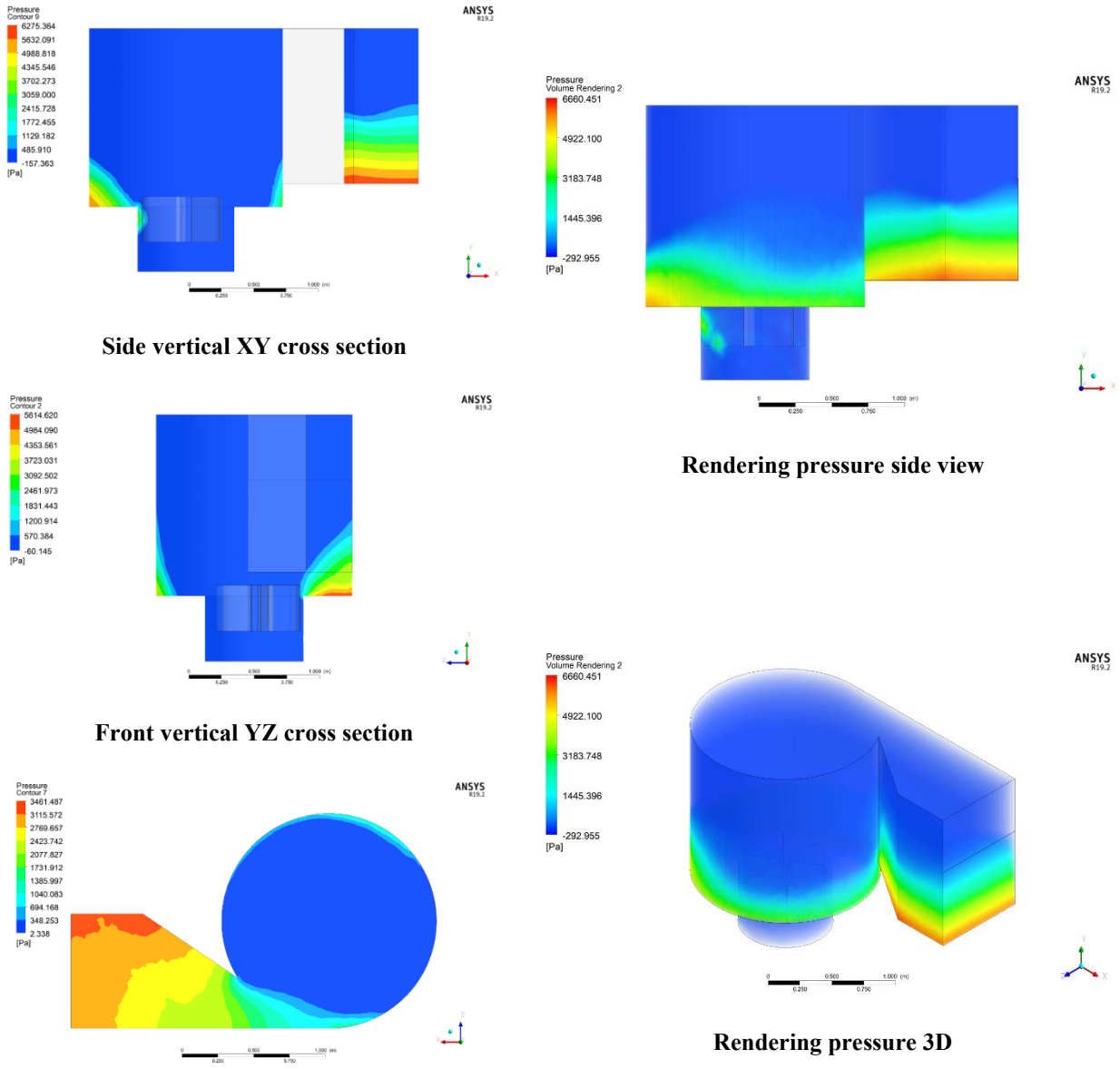

Fig. 13. Pressure distribution of the vortex chamber at 90° blade angle (various cross-sections)

At the 105° angle, the pressure contours exhibit an unfavorable and distorted pattern. Although the maximum pressure reaches 5892.066 Pa, the overall distribution pattern surrounding the blades demonstrates significant distortion (Figure 14). This distortion in the pressure profile is a direct consequence of the previously observed premature flow separation, which severely disrupts the effective transfer of momentum and energy. The flow separation results in a failure to maximize the effective differential pressure drop. Consequently, this increases hydraulic losses and reduces vortex quality, collectively reducing the effectiveness of momentum transfer within the flow. This suboptimal pressure-contour arrangement supports the conclusion that the 105° design should be avoided.

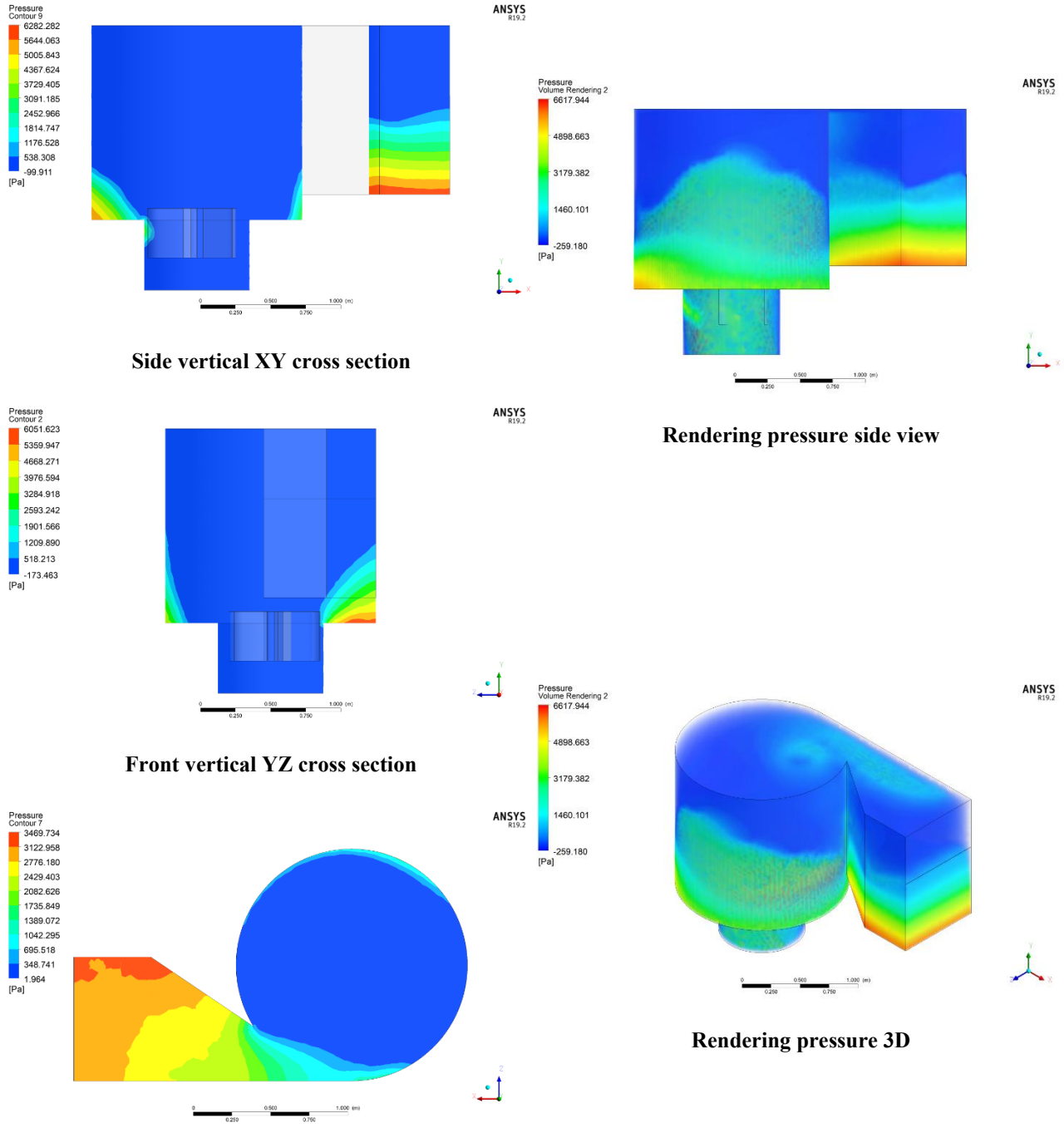

Fig. 14. Pressure distribution in the vortex chamber at 105° blade angle (various cross-sections)

To quantitatively compare the performance of the three configurations, the 90° blade angle shows a significant improvement in hydrodynamic behavior. Compared to the 75° case, the maximum velocity increases by approximately 41.4%, while the pressure distribution becomes more uniform and symmetric. In contrast, although the 105° configuration exhibits the highest peak velocity (4.657 m/s), the presence of flow separation reduces its effectiveness. These results confirm that vortex stability, rather than peak velocity alone, is the dominant factor governing turbine performance.

The hydrodynamic analysis unequivocally reveals that deviation from the optimal 90° angle, whether below or above, demonstrably degrades the performance of the Hydro-Vortex Water Turbine. In the 75° configuration, flow stability constitutes the primary failure mechanism. Although the maximum velocity reached 4.644 m/s, the kinetic energy failed to consolidate into a stable vortex ring, as evidenced by the fragmented velocity contours. This rotational failure directly caused the air nucleus (water volume fraction 0) to become wide and asymmetrical, severely limiting the effective contact area between the fluid and the blades. Concurrently, the pressure pattern exhibits asymmetry, with a peak pressure of 5741.087 Pa, indicating reduced effectiveness in transferring tangential momentum into a consistent pressure differential.

Conversely, at the 105° angle, the failure mechanism was dominated by premature flow separation, as evidenced by the distorted velocity profile (reaching a peak of 4.657 m/s) and the widening of the air nucleus. This distortion resulted in an imbalanced pressure pattern (peak 5892.066 Pa), ultimately increasing hydraulic losses and reducing the turbine's capacity to maintain vortex compactness.

The performance of the HVWT is critically dependent on the blade design's ability to maintain the vortex's structural integrity within the basin (Zainal & Ahmed, 2025). Any deviation in the blade angle from the optimal configuration immediately compromises flow stability. This is initially evidenced by fragmented velocity contours and a broadening of the air nucleus, which fundamentally restricts the effective fluid area available for interaction with the blades (Edirisinghe et al., 2022). The hydrodynamic instability resulting from these non-optimal blade angles ultimately manifests as an asymmetric or distorted pressure pattern around the blades. Mechanically, this prevents the differential pressure gradient required for force generation from being maximized, thereby reducing the overall energy conversion efficiency (Velásquez et al., 2024).

The 90° blade configuration demonstrates its hydrodynamic superiority by establishing an optimal, integrated relationship among the three key parameters (Wu et al., 2021). Rotational flow stability is a fundamental prerequisite that was successfully achieved, with the velocity distribution consistently forming a dense, stable vortex ring (Wang et al., 2023). This stability directly translated into the formation of a slender and focused air nucleus (water volume fraction 0), which is crucial because it ensures that the effective volume of swirling water (1.000 fraction) is maximized for interaction with the vane surfaces, unlike the wide and unfocused air nucleus observed at the other angles (Zamzami et al., 2025b). This stable and uniform flow quality successfully minimized energy dissipation due to turbulence and recirculation observed in the suboptimal configurations.

Achieving high vortex structural integrity yields a symmetric and highly favorable pressure gradient (Zamzami et al., 2025b). Such symmetry indicates a stable flow regime, in which fluid momentum is effectively converted into thrust across the blades, thereby maximizing the extractable differential pressure drop (Qu et al., 2021). Consequently, this configuration is optimal for maintaining and maximizing vortex energy conversion and turbine efficiency.

The pressure distribution analysis provides the definitive mechanical confirmation of the observed flow conditions. The 90° configuration was the only design that generated an optimal and symmetric pressure gradient, with a maximum pressure of 5777.397 Pa effectively concentrated on the pressure side. Conversely, the asymmetric pressure pattern at 75° and the distorted pattern at 105° indicate an ineffective exploitation of fluid pressure (Zheng et al., 2022). Therefore, the synthesis of the results confirms that flow stability and vortex compactness, induced by the optimal angle, are absolute prerequisites for an efficient pressure gradient, forming the primary basis for the recommendation of the optimal configuration in practical applications.

The maximum pressure observed in the 90° configuration (5777.397 Pa) aligns with the theoretical expectation that a stable vortex maintains higher kinetic energy potential. The significant pressure drop to 3.154 Pa on the suction side confirms an efficient momentum transfer, as described by Euler's turbine theorem, where the change in tangential momentum is maximized at this perpendicular orientation compared to the 75° and 105° configurations.

A comparative synthesis of the analyzed configurations reveals a clear parabolic trend in performance relative to the blade angle. At a lower angle (75°), the failure is driven by rotational instability, in which kinetic energy remains fragmented, preventing the formation of a cohesive vortex. As the angle moves toward the 90°

optimum, a clear trend of 'vortex consolidation' is observed, characterized by the simultaneous maximization of velocity symmetry and air nucleus compactness. Beyond this point (105°), the trend reverses due to the dominance of adverse pressure gradients, leading to premature flow separation. This analysis demonstrates that turbine effectiveness is not merely a function of peak velocity, but is governed by the structural integrity of the vortex core, which is highly sensitive to angular deviations from the 90° perpendicular orientation.

By synthesizing the results across all configurations, a generalized relationship between blade angle *(β)* and energy extraction effectiveness can be established. The performance of the HVWT is governed by the 'Vortex Compactness Ratio,' where the stability of the tangential velocity distribution directly dictates the pressure gradient *(∇P)* across the vanes. Our findings suggest that for $\beta < 90°$, the primary limiting factor is the lack of vortex consolidation, leading to fragmented energy zones. Conversely, for $\beta < 90°$, the performance is curtailed by premature flow separation and an expanded air nucleus. Therefore, the optimal energy transfer in a vortex chamber follows a peak-distribution trend centered at the perpendicular orientation (90°), where the fluid's angular momentum is most efficiently converted into mechanical thrust with minimal hydraulic dissipation. This principle suggests that maintaining a symmetric, slender air nucleus is a universal requirement for maximizing the pressure drop *(∇P)* in any gravitational vortex system, serving as a fundamental design heuristic for future turbine optimizations.

4. CONCLUSIONS AND FUTURE WORKS

This study evaluated the influence of blade angle variations (75°, 90°, and 105°) to identify the optimal configuration for improved hydrodynamic performance in ultra-low head applications. The synthesis of numerical results leads to the following conclusions. The 90° configuration exhibits the most favorable combination of pressure and velocity distributions, indicating stable flow behavior under ultra-low-head conditions. It establishes a stable vortex ring (4.376 m/s) and a focused air nucleus, ensuring maximum symmetric differential pressure (5777.397 Pa) for efficient momentum transfer. Deviations from the 90° angle result in significant performance degradation. The 75° configuration fails due to rotational instability and fragmented flow, while the 105° design is limited by premature flow separation and hydraulic distortion, despite higher peak pressures. The results conclusively demonstrate that vortex integrity and symmetry are more critical than peak velocity alone. The six-bladed 90° configuration is recommended as the most effective design for maximizing energy extraction in practical HVWT applications. To further advance the development of the Hydro-Vortex Water Turbine, future studies will include physical prototype testing to validate numerical findings against empirical data and ensure the reliability of observed hydrodynamic trends. A more comprehensive grid-independence study, using a wider range of refinement ratios beyond the current parameters, is planned to further enhance numerical certainty. Further investigation into the correlations among blade curvature, number of blades, and basin geometry is required to establish a more universal design framework for vortex-based energy extraction.

Author Contributions

Conceptualization, methodology, validation, and formal analysis, S.E.S, Z. and A.A.; investigation, software, resources, data curation, visualization, and writing - original draft preparation, S.E.S, Z. and A.A.; writing – review and editing, Z., A.A., S., S.E.S. and A.S. All authors have read and agreed to the published version of the manuscript.

Funding

This publication was made possible by a grant from the Research Fund of the Ministry of Research, Technology, and Education, Republic of Indonesia, and LPPM Universitas Syiah Kuala; the financial support is greatly appreciated (Number: 094/E5/PG.02.00.PL/2024; Number: 589/UN11.2.1/PG.01.03/SPK/DRTPM/2024).

Conflicts of Interest

The authors declare no conflict of interest.

REFERENCES

Domfeh, M. K., Gyamfi, S., Amo-Boateng, M., Andoh, R., Ofosu, E. A., & Tabor, G. (2020). Free surface vortices at hydropower intakes: A state-of-the-art review. *Scientific African, 8*, Article e00355. https://doi.org/10.1016/j.sciaf.2020.e00355

Edirisinghe, D. S., Yang, H. S., Gunawardane, S. D. G. S. P., & Lee, Y. H. (2022). Enhancing the performance of gravitational water vortex turbine by flow simulation analysis. *Renewable Energy, 194*, 163–180. https://doi.org/10.1016/j.renene.2022.05.053

Firoozi, A. A., Hejazi, F., & Firoozi, A. A. (2024). Advancing wind energy efficiency: A systematic review of aerodynamic optimization in wind turbine blade design. *Energies, 17*(12), Article 2919. https://doi.org/10.3390/en17122919

Frant, M., Kozakiewicz, A., & Kachel, S. (2020). Analysis of impact of gust angle and velocity on the position of stagnation point. *Advances in Science and Technology Research Journal, 14*(4), 49–57. https://doi.org/10.12913/22998624/123006

Gayen, D., Chatterjee, R., & Roy, S. (2024). A review on environmental impacts of renewable energy for sustainable development. *International Journal of Environmental Science and Technology, 21*(5), 5285–5310. https://doi.org/10.1007/s13762-023-05380-z

Hou, X., Yuan, J., Fu, Y., Wang, P., Zhang, P., & He, N. (2024). Submerged vortex morphology and pressure fluctuation characteristics in intake sump. *Journal of Applied Fluid Mechanics, 17*(10), 2100–2114. https://doi.org/10.47176/jafm.17.10.2640

Ibrahim, A. A., Elbaz, A. M., Melani, P. F., Mohamed, O. S., & Bianchini, A. (2022). Power augmentation of Darrieus wind turbine blades using trapped vortex cavity. *Journal of Wind Engineering and Industrial Aerodynamics, 223*, Article 104949. https://doi.org/10.1016/j.jweia.2022.104949

Kabat, S. R., Panigrahi, C. K., Ganthia, B. P., Barik, S. K., & Nayak, B. (2022). Implementation and analysis of mathematical modeled drive train system in type III wind turbines using computational fluid dynamics. *Advances in Science and Technology Research Journal, 16*(1), 180–189. https://doi.org/10.12913/22998624/144753

Kan, K., Xu, Y., Li, Z., Xu, H., Chen, H., Zi, D., Gao, Q., & Shen, L. (2023). Numerical study of instability mechanism in the air-core vortex formation process. *Engineering Applications of Computational Fluid Mechanics, 17*(1), Article 2156926. https://doi.org/10.1080/19942060.2022.2156926

Khoshkalam, N., Najafi, A. F., Rahimian, M. H., & Magagnato, F. (2020). Numerical study on air-core vortex: Analysis of generation mechanism. *Archive of Applied Mechanics, 90*(1), 1–16. https://doi.org/10.1007/s00419-019-01596-z

Li, B., Zhou, D. L., Wang, Y., Shuai, Y., Liu, Q. Z., & Cai, W. H. (2020). The design of a small lab-scale wind turbine model with high performance similarity to its utility-scale prototype. *Renewable Energy, 149*, 435–444. https://doi.org/10.1016/j.renene.2019.12.060

Li, G., Wu, G., Tan, L., & Fan, H. (2023). A review: Design and optimization approaches of the Darrieus water turbine. *Sustainability, 15*(14), Article 11308. https://doi.org/10.3390/su151411308

Lodhi, S. K., Hussain, H. K., & Gill, A. (2024). Renewable energy technologies: Present patterns and upcoming paths in ecological power production. *Global Journal of Universal Studies, 1*(1), 108–131. https://doi.org/10.70445/gjus.1.1.10

Maika, N., Lin, W., & Khatamifar, M. (2023). A review of gravitational water vortex hydro turbine systems for hydropower generation. *Energies, 16*(14), Article 5394. https://doi.org/10.3390/en16145394

Maisuria, M., Ratadiya, L., & Patel, A. (2024). Computational investigation and optimization of the bulb turbine for ultra-low head application. *Renewable Energy, 230*, Article 120876. https://doi.org/10.1016/j.renene.2024.120876

Masoodi, F. A., & Goyal, R. (2021). Efficacy of ancillary fluid injection technique for mitigation of vortex rope in hydraulic turbines: A review. *Materials Today: Proceedings, 47*, 3043–3053. https://doi.org/10.1016/j.matpr.2021.05.618

Pędzisz, I., Magryta, P., & Pietrykowski, K. (2024). Computational fluid dynamics studies of a vertical axis wind turbine with a variable swept area. *Advances in Science and Technology Research Journal, 18*(2), 1–13. https://doi.org/10.12913/22998624/185255

Permana, A. S., & Potipituk, C. (2024). Harmonizing power generation and environmental conservation through micro-hydro systems. W: *Turbulence & Energy Laboratory Annual Conference* (s. 1–34). Springer Nature Switzerland. https://doi.org/10.1007/978-3-031-73486-1_1

Qu, X., Zhang, Y., Lu, X., Zhu, J., & Zhang, Y. (2021). Unsteady fluidic oscillators for active controlling boundary layer separation in an ultra-high-lift low-pressure turbine. *Aerospace Science and Technology, 119*, Article 107130. https://doi.org/10.1016/j.ast.2021.107130

Seng, W. K., & Tanjong, S. J. (2025). Investigation on blade angles effect on micro-gravitational water vortex system via simulation and experimental analysis. *Pena Journal of Flow Dynamics, 1*(1), 13–27. https://doi.org/10.37934/pjfd.1.1.1327

Shamsuddeen, M. M., Ma, S. B., Park, N. H., Kim, K. M., & Kim, J. H. (2023). Design analysis and optimization of a hydraulic gate turbine for power production from ultra-low head sites. *Energy, 275*, Article 127371. https://doi.org/10.1016/j.energy.2023.127371

Sharma, A., Hettiarachchi, S., & Wasko, C. (2021). Estimating design hydrologic extremes in a warming climate: Alternatives, uncertainties and the way forward. *Philosophical Transactions of the Royal Society A, 379*(2195), Article 20190623. https://doi.org/10.1098/rsta.2019.0623

Sonawat, A., Kim, S. J., Yang, H. M., Choi, Y. S., Kim, K. M., Lee, Y. K., & Kim, J. H. (2020). Positive displacement turbine – A novel solution to the pressure differential control valve failure problem and energy utilization. *Energy, 190*, Article 116400. https://doi.org/10.1016/j.energy.2019.116400

Sukadana, I. G. K., Suarda, M., Widiarta, I. P., & Danus, I. (2024). CFD (Computational Fluid Dynamics) simulation of hydrodynamic vortex turbine performance: Influence of notch angle variation on flow patterns and efficiency. *Natural Sciences Engineering and Technology Journal, 4*(2), 336–351. https://doi.org/10.37275/nasetjournal.v4i2.56

Ullah, R., Cheema, T. A., Saleem, A. S., Ahmad, S. M., Chattha, J. A., & Park, C. W. (2020). Preliminary experimental study on multi-stage gravitational water vortex turbine in a conical basin. *Renewable Energy, 145*, 2516–2529. https://doi.org/10.1016/j.renene.2019.06.096

Varga, M., Velásquez, L., Rubio-Clemente, A., Ramón Valencia, B., & Chica, E. (2025). Experimental analysis of gravitational vortex turbine made from natural fibers. *Materials, 18*(10), Article 2352. https://doi.org/10.3390/ma18102352

Velásquez, L., Rubio-Clemente, A., & Chica, E. (2024). Numerical and experimental analysis of vortex profiles in gravitational water vortex hydraulic turbines. *Energies, 17*(14), Article 3543. https://doi.org/10.3390/en17143543

Wang, C., Lin, W., Lin, X., Wu, T., Meng, Z., Cai, A., Xu, Z., Li, Y., & Feng, F. (2024). The influence of angle of attack on the icing distribution characteristics of DU97 blade airfoil surface for wind turbines. *Coatings, 14*(2), Article 160. https://doi.org/10.3390/coatings14020160

Wang, X., Du, P., Yao, L., Zou, Z., & Zeng, F. (2023). Uncertainty analysis of measured geometric variations in turbine blades and impact on aerodynamic performance. *Chinese Journal of Aeronautics, 36*(6), 140–160. https://doi.org/10.1016/j.cja.2023.03.041

Wu, J., Jin, Y., Hao, Y., & Lu, J. (2021). Identification of the control factors affecting water quality variation at multi-spatial scales in a headwater watershed. *Environmental Science and Pollution Research, 28*(9), 11129–11141. https://doi.org/10.1007/s11356-020-11352-4

Zainal, H. M., & Ahmed, O. K. (2025). Performance assessment of water vortex power plant: Effect of material type and blade number. *Results in Engineering, 26*, Article 104775.

Zamzami, Z., Akhyar, A., Sofyan, S. E., Suriadi, S., & Khairil, K. (2025a). A review of vortex water turbine design for sustainable energy generation (principles, optimization, and validation). *Energy Conversion and Management: X, 26*, 1–126. https://doi.org/10.1016/j.ecmx.2025.100895

Zamzami, Z., Akhyar, A., Suriadi, S., Sofyan, S. E., Khairil, K., Hasannuddin, T., & Yassir, Y. (2025b). The influence of water velocity and blade number variation on the performance of water vortex turbines. *Multidisciplinary Science Journal, 8*(1). https://doi.org/10.31893/multiscience.2026068

Zheng, G., Gu, Z., Xu, W., Lu, B., Li, Q., Tan, Y., Wang, C., & Li, L. (2022). Gravitational surface vortex formation and suppression control: A review from hydrodynamic characteristics. *Processes, 11*(1), Article 42. https://doi.org/10.3390/pr11010042